

RESONANCE IN FORCED FLUX TRANSPORT DYNAMOS

Peter A. Gilman and Mausumi Dikpati

*High Altitude Observatory, National Center for Atmospheric Research, 3080 Center Green,
Boulder, CO 80307-3000.*

`gilman@ucar.edu, dikpati@ucar.edu`

ABSTRACT

We show that simple 2 and 3-layer flux-transport dynamos, when forced at the top by a poloidal source term, can produce a widely varying amplitude of toroidal field at the bottom, depending on how close the meridional flow speed of the bottom layer is to the propagation speed of the forcing applied above the top layer, and how close the amplitude of the α -effect is to two values that give rise to a resonant response. This effect should be present in this class of dynamo model no matter how many layers are included. This result could have implications for the prediction of future solar cycles from the surface magnetic fields of prior cycles. It could be looked for in flux-transport dynamos that are more realistic for the Sun, done in spherical geometry with differential rotation, meridional flow and α -effect that vary with latitude and time as well as radius. Because of these variations, if resonance occurs, it should be more localized in time, latitude and radius.

Subject headings: Sun: solar dynamo

1. INTRODUCTION

Dikpati et al (2006) first used a flux transport dynamo calibrated to the Sun (Dikpati et al 2004) to simulate and predict solar cycle peaks from the record of past surface magnetic field patterns. This was done mathematically by forcing the dynamo equations at the top boundary, with a forcing function derived from past surface magnetic fields. Flux transport dynamos, and indeed all dynamos, have their own unforced, usually complex frequencies of excitation that are commonly found by treating the dynamo equations as an eigenvalue problem. Many naturally occurring and man-made systems have such properties.

When a physical system that has natural frequencies is excited by external forcing whose own frequency is close to one of the natural ones, there can be resonance produced—that is,

the system will be excited strongly by the forcing compared to the case where the forcing frequency is not close to a natural one. The purpose of this paper is to explore the possibility of resonance in flux-transport dynamos relevant to the solar cycle.

In flux transport dynamos, there are several physical properties that help determine the unforced frequencies of the system. These include differential rotation, meridional circulation, the so-called α -effect, or kinetic helicity, and turbulent magnetic diffusion. It is now well established (Dikpati and Charbonneau, 1999) that unless the magnetic diffusivity is very large, meridional flow at the bottom of the dynamo layer is primarily responsible for the real part of the natural frequency of the dynamo, which determines the speed with which induced toroidal and poloidal fields near the bottom migrate toward the equator. Therefore the closeness of the frequency of forcing at the top to the speed of the flow at the bottom could help determine how much dynamo response there is.

Since the forcing at the top is created by emergence of concentrated magnetic flux from the bottom, in the form of active regions, and the rate of movement of the zone where active regions are found moves toward the equator (not coincidentally) at a rate close to the meridional flow speed near the bottom, we might expect the conditions for resonance to occur in the bottom layer to be favorable. On the other hand, we know from observations (Ulrich, 2010 and references therein) that the meridional flow at the top of the convection zone is toward the poles, opposite to the propagation of the surface forcing as well as 5-10 times faster. Thus we should not expect resonance to occur near the surface.

It is also well known (Ulrich 2010 and references therein) that the meridional circulation varies with time. This time variation is now being incorporated into a flux-transport dynamo used for prediction by Dikpati and colleagues. In the 2006 prediction, meridional circulation generally was kept fixed in time. Dikpati et al (2006), Dikpati and Gilman (2006) recognized that such time variations could be important, but felt they lacked sufficient knowledge of its variations to include them. They adjusted the time-independent meridional flow amplitude to give the average period of the past solar cycles, and stretched or compressed all the surface forcing data to the same period, to avoid any artificial or non-physical mismatches between the natural dynamo period and the period of the forcing.

But there can also in principle in the Sun be real differences between the period of the top forcing that was created by the previous cycle, and the frequency of equatorward propagation associated with the meridional flow speed at the bottom. In dynamos forced at the top with a specified period, the amplitude of the induced fields within the dynamo domain will be affected by this frequency difference. The model we present here in effect studies how this amplitude is affected, by treating the meridional flow at the bottom as a free parameter while keeping the frequency of the top forcing fixed.

In the real sun, the cycle period varies from cycle to cycle, as does the speed of the meridional flow and its profile with latitude. Ultimately it is highly desirable to include both such variations. This can be done by use of data assimilation techniques applied to both the surface forcing and meridional flow variations. As we said above, Dikpati and colleagues are doing that now. When that is accomplished, they may find that resonance plays some role. In this paper, we anticipate that possibility and focus on possible resonances by using a much simpler dynamo model than used in Dikpati and Gilman (2006), namely one that has no more than two three layers in the radial direction.

Such an approach has the advantage of speed while retaining important physical processes. But such a simple model would have little value as a tool for prediction, because it could not be calibrated well in detail to the sun, since it would have few degrees of freedom. It also may overestimate the importance of resonance for the same reason. The cautions expressed in Roald (1998) about the limits of dynamo models with one or two layers are well taken. Nevertheless, since the forced dynamo problem has only begun to be studied, particularly in the solar case, using a really simple model initially may give useful guidance about what to look for with a more realistic version. It is in this spirit that we report on these calculations here.

Resonance has been studied in dynamos previously, but the literature is small. General examples include Strauss (1986) and Reshetnyak (2010). Resonance in the geodynamo has been studied by Stefani and Gerberth (2005) and Fischer et al (2008). Studies for disks and galaxies include Chiba (1991), Schmitt and Rüdiger (1992), Kuzanyan and Sokoloff (1993), and Moss (1996). We have not located any previous studies specific to the Sun in which resonance has been explicitly identified and highlighted. However in all these areas there are almost certainly model studies in which some form of resonance is playing a role, but has not been brought out in the analysis of results. Any dynamo in which inputs such as flow fields or turbulent parameters such as the α -effect are allowed to vary with time, either imposed or by nonlinearities internal to the system, such as 'quenching', could display behavior related to resonance.

2. DYNAMO EQUATIONS AND PHYSICS

We start from the standard flux-transport dynamo equations in vector form that include differential rotation, meridional circulation, turbulent magnetic diffusivity, and allow for an inhomogeneous top boundary condition. In vector-invariant form, this equation is given by

$$\frac{\partial \mathbf{B}}{\partial t} = \nabla \times (\mathbf{v} \times \mathbf{B}) + \nabla \times (\alpha \mathbf{B}) - \nabla \times (\eta \nabla \times \mathbf{B}) \quad (1)$$

In this equation, \mathbf{B} is the vector magnetic field, \mathbf{v} is the vector velocity, α is the well known alpha-effect, and η is the turbulent magnetic diffusivity.

In addition, \mathbf{B} must satisfy the divergence-free condition $\nabla \cdot \mathbf{B} = 0$. This can be a problem numerically if we are solving for the three vector components of the magnetic field directly. But satisfaction of this condition is guaranteed if instead we define the magnetic field in terms of vector potential functions. There are at least two possible ways to do this. The standard one from electromagnetic theory is to let $\mathbf{B} = \nabla \times \mathbf{A}$, 'factor out' a curl operator from the whole equation. The resulting equation is given by

$$\frac{\partial \mathbf{A}}{\partial t} = \mathbf{v} \times \nabla \times \mathbf{A} + \alpha \nabla \times \mathbf{A} - \eta \nabla \times \nabla \times \mathbf{A} \quad (2)$$

Equations (1) and (2) are quite general, including parameters and variables that can vary with all three space dimensions, in any coordinate system. Here we simplify the problem to an infinite plane layer and use cartesian geometry. We restrict the system further by assuming all quantities are independent of one coordinate in the plane, which we take to be the y coordinate. We identify this coordinate with longitude on the sun, so that in the cartesian system the $x - z$ plane corresponds to the meridional plane on the sun. The coordinate x then corresponds to colatitude and z to radius. Then in this frame, we take the velocities to be v, u, w in the x, y, z directions respectively. To describe the magnetic field in this system requires only two variables, namely the y components of the toroidal field and the poloidal potential. We denote these scalar quantities by B and A respectively. The magnetic diffusivity is denoted by η . Then the vector system in Equations (1) and (2) reduces to a pair of scalar equations for A and B as follows

$$\frac{\partial A}{\partial t} = -v \frac{\partial A}{\partial x} - w \frac{\partial A}{\partial z} + \alpha B + \eta \left(\frac{\partial^2}{\partial x^2} + \frac{\partial^2}{\partial z^2} \right) A \quad (3)$$

$$\begin{aligned} \frac{\partial B}{\partial t} = & -\frac{\partial(vB)}{\partial x} - \frac{\partial(wB)}{\partial z} - \frac{\partial}{\partial x} \left(\alpha \frac{\partial A}{\partial x} \right) - \frac{\partial}{\partial z} \left(\alpha \frac{\partial A}{\partial z} \right) \\ & + \frac{\partial u}{\partial z} \frac{\partial A}{\partial x} - \frac{\partial u}{\partial x} \frac{\partial A}{\partial z} + \frac{\partial}{\partial x} \left(\eta \frac{\partial B}{\partial x} \right) + \frac{\partial}{\partial z} \left(\eta \frac{\partial B}{\partial z} \right) \end{aligned} \quad (4)$$

We simplify the problem further by restricting all coefficients in equations (3) and (4) to be independent of x . This allows for separation of variables. To achieve this we must

require $w = 0$ so that v can be independent of x , and we must allow u to be either a function of x (latitude) only, or a function of z (radius) only. There is evidence (Dikpati et al 2005) that the latitude gradient of rotation is more important than the radial gradient in the flux transport dynamos that best simulate solar cycles, so in this study we restrict ourselves to consideration of the latitude gradient. The diffusivity η and the α -effect are also taken to be independent of x . Equations (3) and (4) then reduce to

$$\frac{\partial A}{\partial t} = -v \frac{\partial A}{\partial x} + \alpha B + \eta \left(\frac{\partial^2}{\partial x^2} + \frac{\partial^2}{\partial z^2} \right) A \quad (5)$$

$$\begin{aligned} \frac{\partial B}{\partial t} = & -v \frac{\partial B}{\partial x} - \alpha \frac{\partial^2 A}{\partial x^2} - \frac{\partial}{\partial z} \left(\alpha \frac{\partial A}{\partial z} \right) \\ & - \frac{\partial u}{\partial x} \frac{\partial A}{\partial z} + \eta \frac{\partial^2 B}{\partial x^2} + \frac{\partial}{\partial z} \left(\eta \frac{\partial B}{\partial z} \right) \end{aligned} \quad (6)$$

There are a variety of boundary conditions that could be chosen for the top and bottom of the infinite plane layer. Consistent with solar conditions, we take the bottom to be a perfect conductor, and therefore require $A = 0$ there. B in that case is determined internally. For the top there are four plausible alternatives: perfect conductor ($A = 0$ again); insulator with no forcing ($B = 0$ and A matched to potential field above); forcing in potential at top ($A = A_F$) and $B = 0$ or determined internally. We make choices among these boundary conditions when we derive the 1- and 2-layer equations in the next section.

In preparation for these derivations, we simplify the dynamo equations further by taking $\frac{\partial u}{\partial x} = s, v, \alpha, \eta$ all independent of x , and assuming all variables have solutions of the form $e^{i(kx - \omega t)}$ equations (5) and (6) reduce to

$$-i\omega A = -ikvA + \alpha B + \eta \left(-k^2 + \frac{\partial^2}{\partial z^2} \right) A \quad (7)$$

$$-i\omega B = -ikvB + k^2 \alpha A - \frac{\partial}{\partial z} \left(\alpha \frac{\partial A}{\partial z} \right) - s \frac{\partial A}{\partial z} - k^2 B + \frac{\partial}{\partial z} \left(\eta \frac{\partial B}{\partial z} \right) \quad (8)$$

3. REDUCTION TO ONE, TWO AND THREE LAYER MODELS

Before developing 1, 2 and 3-layer dynamo equations in detail, we first describe schematically what variables and parameters are retained in these cases. These are summarized graphically in Figure 1. For all three cases, it is possible to specify boundary values of the

variables in addition to their values within each layer. We denote values at the top by a subscript T and at the bottom by a subscript B . The boundary conditions shown correspond to a perfectly conducting bottom and an insulating or vacuum top with poloidal forcing A_F . In the 2 and 3-layer cases, we can also specify values of the variables at the interface between the upper and lower layers, namely the average of the values above and below. In some studies, the variables are allowed to vary with the vertical coordinate within the layer. Here they vary in the vertical only from layer to layer. Some readers may prefer the term 'level' to that of 'layer' to describe our model.

Schematic definition of 1,2,3 layer models for flux–transport dynamo

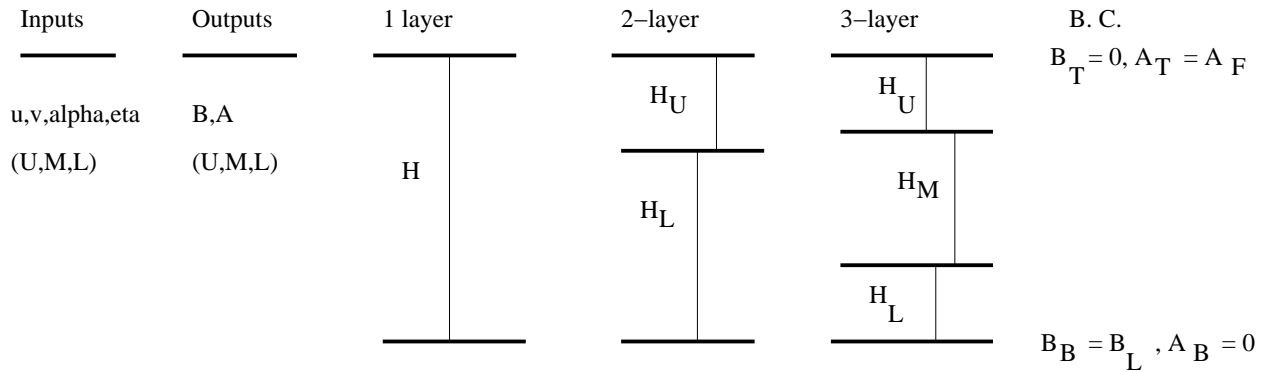


Fig. 1.— Schematic layout of parameters and variables for one,two and three layer models to be used. Leftmost column lists the inputs to the model for each layer, in particular, differential rotation u , meridional circulation v , α -effect and magnetic diffusivity η . Next column lists the outputs, namely toroidal field B and poloidal potential A . The next three columns define the layer thicknesses H respectively for one, two and three layer models. The rightmost column lists the boundary conditions used at the top and bottom of the dynamo domain. In all cases, the subscripts U, M, L refer respectively to the upper, middle, and lower layers.

On the left of Figure 1 are shown the variables B, A and the parameters u, v, α, η for each layer in the model, denoted by the subscripts U, M, L for three layers, U, L for two layers, and unsubscripted for the 1-layer version. The whole depth of the dynamo domain is taken to have a thickness H , no matter how many layers it is subdivided into.

4. 1-LAYER MODEL EQUATIONS AND RESULTS

We now use the boundary conditions defined in Figure 1 to evaluate the vertical derivatives in equations (7) and (8). With rearrangements to put only forcing terms on the right hand sides, these equations become

$$[-i(\omega - kv) + \eta(k^2 + \frac{8}{H^2})]A - \alpha B = \frac{4\eta}{H^2}A_F \quad (9)$$

$$-\alpha(\frac{8}{H^2} + k^2)A + [-i(\omega - kv) + \eta(k^2 + \frac{4}{H^2})]B = -(\frac{4\alpha}{H^2} + \frac{s}{H})A_F \quad (10)$$

We can reduce the number of parameters to take account of by making equations (9) and (10) dimensionless, by using H as the length scale, H^2/η as the time scale and recognize that B/A scales as H . Then velocities and α scale as η/H and equations (9) and (10) become

$$[-i(\omega - kv) + k^2 + 8]A - \alpha B = 4A_F \quad (11)$$

$$-\alpha(k^2 + 8)A + [-i(\omega - kv) + k^2 + 4]B = -(4\alpha + s)A_F \quad (12)$$

We find solutions to equations (11) and (12) from standard linear equation theory. In the case with no forcing, there are solutions only if the (2×2) determinant DT of the coefficients vanishes. This requires that both the real and imaginary parts of DT be zero. DT is given by

$$DT = [-i(\omega - kv) + k^2 + 8][-i(\omega - kv) + k^2 + 4] - \alpha^2(k^2 + 8) = 0, \quad (13)$$

This yields a solution for ω in terms of the mode wavenumber k and the meridional flow v and α -effect, given by

$$\omega = kv - i(k^2 + 6 \pm [(k^2 + 6)^2 + (k^2 + 8)(\alpha^2 - (k^2 + 4))]^{1/2}) \quad (14)$$

When the factor multiplying i in equation (14) is real, then (14) yields modes that propagate at the speed of the meridional flow, and either grow or decay with time. One growing mode is assured if $k^2 < \alpha^2 - 4$, so if the latitudinal scale of the mode is sufficiently large, a growing dynamo mode results. This is a form of flux-transport dynamo, but one in which differential rotation plays no role, even though it is present. This is true only of

the one-layer model; with two or more layers, differential rotation does play a role in the unforced dynamos.

When $k^2 > \alpha^2 - 4$ then there are either all decaying modes, or oscillatory modes that propagate at speeds different from the meridional flow speed. We can think of the condition $k^2 = \alpha^2 - 4$ as the threshold for dynamos to occur.

In the case with forcing A_F at (real) frequency ω_r , bounded solutions to equations (11) and (12) exist only if the determinant DT does not vanish. In this case, the solutions for B and A in terms of A_F are given by

$$B = (k^2 + 8 + i(4\alpha + s)(\omega - kv))A_F/DT \quad (15)$$

$$A = (4A_F + \alpha B)/[-i(\omega - kv) + k^2 + 8] \quad (16)$$

From equation (15) for the toroidal field B we can see immediately that the toroidal field induced in response to the poloidal forcing A_F is largest when DT is smallest, and is unbounded when $DT = 0$. Therefore the system experiences resonance, when the frequency of the forcing equals the 'frequency' kv associated with the meridional flow and the wavenumber of the forcing equals $(\alpha^2 - 4)^{1/2}$. Note that this is the same point in parameter space where there are neutral dynamo waves as found from equation (13). Just as in resonant systems generally, here the natural frequency of the system and the frequency of the forcing are the same. So the presence of resonance requires an α -effect, but from equation (15) it does not require a differential rotation. The resonance in this 1-layer model is independent of the sign of the α -effect. It is well known that α^2 dynamos can have propagating unstable dynamo modes, so resonance is possible in such systems without the effect of differential rotation. In models with two or more layers, resonance does involve differential rotation.

What is the relevance of this resonance phenomenon to the solar cycle? We know that at the top of the convection zone, the meridional flow and surface poloidal forcing are propagating in opposite directions, with the poleward meridional flow being an order of magnitude greater. Therefore in this domain the dynamo should be far from resonance. But at the bottom, the meridional flow is toward the equator, and has a speed similar to the propagation speed of the surface poloidal source. Therefore if the surface poloidal source can be 'felt' near the bottom of the convection zone, resonance might occur. A 1-layer dynamo model is inadequate to test for this possibility, so we must use a model with at least two layers.

5. 2 AND 3-LAYER MODEL EQUATIONS

5.1. 2-LAYER EQUATIONS

For the 2-layer model equations, we proceed in the same way as with the 1-layer equations. But here, as listed in Figure 1, most parameters have different values for the upper and lower layers. But for simplicity and to be able to achieve separation of variables, we keep the y (latitudinal) gradient s of the east-west (rotational) flow the same in both layers. Then the dimensional 2-layer equations become

$$[-i(\omega - kv_U) + \eta_U(k^2 + 6/H_U^2)]A_U - \alpha_U B_U - 2\eta_U A_L/H_U^2 = 4\eta_U A_F/H_U^2 \quad (17)$$

$$\begin{aligned} -(\alpha_U(k^2 + 6/H_U^2) + s/2H_U)A_U + [-i(\omega - kv_U) + \eta_U(k^2 + 6/H_U^2)]B_U + (2\alpha_U/H_U^2 - s/2H_U)A_L \\ - 2\eta_U B_L/H_U^2 = -(4\alpha_U/H_U^2 + s/H_U)A_F \end{aligned} \quad (18)$$

$$-2(\eta_L/H_L^2)A_U + [-i(\omega - kv_L) + \eta_L(k^2 + 6/H_L^2)]A_L - \alpha_L B_L = 0 \quad (19)$$

$$\begin{aligned} (2\alpha_L/H_L^2 + s/2H_L)A_U - 2\eta_L/H_L^2 B_U \\ + [-\alpha_L(k^2 + 6/H_L^2) + s/2H_L]A_L \\ + [-i(\omega - kv_L) + \eta_L(k^2 + 2/H_L^2)]B_L = 0 \end{aligned} \quad (20)$$

By inspection, we can see that the layers are coupled by processes involving diffusion, differential rotation and the α -effect. To render the system dimensionless in this case, we use H for the length scale and H^2/η_U for the time scale. We also introduce the parameters $P_{vL}, P_{\alpha L}, P_{\eta L}$ respectively for the ratios $v_L/v_U, \alpha_L/\alpha_U, \eta_L/\eta_U$. We also define $D_U = H_U/H$ and $D_L = H_L/H$. Then $D_U + D_L = 1$. With these definitions and evaluating the z derivatives in equations (7) and (8), we get four equations for the toroidal field and poloidal potential of the two layers. In dimensionless form these equations are

$$[-i(\omega - kv_U) + k^2 + 6/D_U^2]A_U - \alpha_U B_U - 2A_L/D_U^2 = 4A_F/D_U^2 \quad (21)$$

$$\begin{aligned}
 & -(\alpha_U(k^2 + 6/D_U^2) + s/2D_U)A_U + [-i(\omega - kv_U) + k^2 + 6/D_U^2]B_U + (2\alpha_U/D_U^2 - s/2D_U)A_L \\
 & \quad -2B_L/D_U^2 = -(4\alpha_U/D_U^2 + s/D_U)A_F
 \end{aligned} \tag{22}$$

$$-2(P_{\eta L}/D_L^2)A_U + [-i(\omega - kP_{vL}v_U) + (k^2 + 6/D_L^2)P_{\eta L}]A_L - P_{\alpha L}\alpha_U B_L = 0 \tag{23}$$

$$\begin{aligned}
 & (2P_{\alpha L}\alpha_U/D_L^2 + s/2D_L)A_U - 2(P_{\eta L}/D_L^2)B_U \\
 & \quad + [-P_{\alpha L}\alpha_U(k^2 + 6/D_L^2) + s/2D_L]A_L \\
 & \quad + [-i(\omega - kP_{vL}v_U) + (k^2 + 2/D_L^2)P_{\eta L}]B_L = 0
 \end{aligned} \tag{24}$$

By analogy with the 1-layer system, in the 2-layer case we should expect resonance to be found near where the (4X4) determinant of the coefficients in equations (17)-(20) vanishes. In the homogeneous case ($A_F = 0$) this determinant is a quartic equation for the complex eigenfrequency ω of the dynamo of the 2-layer system. Being a 4th order system, we can not in general find closed or simple algebraic forms for either the amplitudes of the response to the top forcing, or the phase speed and growth rate of the unforced dynamo. But only small programs are necessary to get results.

For the case with forcing, we find the amplitudes and phases of A_U, A_L, B_U, B_L in terms of the amplitude and phase of A_F by application of Cramers rule (refs). We apply Cramers rule to equations (21)-(24) defined in symbolic form as

$$c_{11}A_U + c_{12}B_U + c_{13}A_L + c_{14}B_L = F_1A_F \tag{25}$$

$$c_{21}A_U + c_{22}B_U + c_{23}A_L + c_{24}B_L = F_2A_F \tag{26}$$

$$c_{31}A_U + c_{32}B_U + c_{33}A_L + c_{34}B_L = 0 \tag{27}$$

$$c_{41}A_U + c_{42}B_U + c_{43}A_L + c_{44}B_L = 0 \tag{28}$$

in which all of the $c_{i,j}$ coefficients and F_1, F_2 are defined by matching terms in equations (25)-(28) with their counterparts respectively in equations (21)-(24), so that $c_{14} = 0$ and

$c_{32} = 0$. Then to make Cramers rule work, we must have the determinant of the coefficients in equations (25)-(28) not vanish. But where it approaches zero is where in the parameter space we should expect resonance to occur, since this determinant is the denominator for the solutions of equations (25)-(28) found by Cramers rule.

5.2. 3-LAYER EQUATIONS

How would the results we have obtained change if we added another layer to the system? If the results concerning resonance are similar, it gives us more confidence that the same phenomenon may occur in much more realistic systems with many layers in the vertical. If not, then the results obtained above have much more limited significance for the general case. With three layers, the number of equations to be solved expands to six. These are given by

$$[-i(\omega - kv_U) + k^2 + \frac{6}{D_U^2}]A_U - \alpha_U B_U - \frac{2}{D_U^2}A_M = \frac{4}{D_U^2}A_F \quad (29)$$

$$\begin{aligned} [-\alpha_U(k^2 + \frac{6}{D_U^2}) - \frac{s}{2D_U}]A_U + [-i(\omega - kv_U) + k^2 + \frac{6}{D_U^2}]B_U + (\frac{2\alpha_U}{D_U^2} - \frac{s}{2D_U})A_M \\ - \frac{2}{D_U^2}B_M = -(\frac{4\alpha_U}{D_U^2} + \frac{s}{D_U})A_F \end{aligned} \quad (30)$$

$$-\frac{2P_{\eta M}}{D_M^2}A_U + [-i(\omega - kv_U P_{vM}) + P_{\eta M}(k^2 + \frac{4}{D_M^2})]A_M - \alpha_U P_{\alpha M}B_M - \frac{2P_{\eta M}}{D_M^2}A_L = 0 \quad (31)$$

$$\begin{aligned} [\frac{2\alpha_U P_{\alpha M}}{D_M^2} + \frac{s}{2D_M}]A_U - \frac{2P_{\eta M}}{D_M^2}B_U - \alpha_U P_{\alpha M}(k^2 + \frac{4}{D_M^2})A_M \\ + [-i(\omega - kv_U P_{vM}) + P_{\eta M}(k^2 + \frac{4}{D_M^2})]B_M + [\frac{2\alpha_U P_{\alpha M}}{D_M^2} - \frac{s}{2D_M}]A_L - \frac{2P_{\eta M}}{D_M^2}B_L = 0 \end{aligned} \quad (32)$$

$$-\frac{2P_{\eta L}}{D_L^2}A_M + [-i(\omega - kv_U P_{vL}) + P_{\eta L}(k^2 + \frac{6}{D_L^2})]A_L - \alpha_U P_{\alpha L}B_L = 0 \quad (33)$$

$$\frac{s}{2D_L}A_U - \frac{2\alpha_U P_{\alpha L}}{D_L^2}A_M - \frac{2P_{\eta L}}{D_L^2}B_M + [-\alpha_U P_{\alpha L}(k^2 + \frac{6}{D_L^2}) + \frac{s}{2D_L}]A_L$$

$$+[-i(\omega - kv_U P_{vL}) + P_{\eta L}(k^2 + \frac{2}{D_L^2})]B_L = 0 \quad (34)$$

Similar to equations (25)-(28) above, equations (29)-(34) can be written in symbolic form as

$$c_{11}A_U + c_{12}B_U + c_{13}A_M + c_{14}B_M + c_{15}A_L + c_{16}B_L = F_1A_F \quad (35)$$

$$c_{21}A_U + c_{22}B_U + c_{23}A_M + c_{24}B_M + c_{25}A_L + c_{26}B_L = F_2A_F \quad (36)$$

$$c_{31}A_U + c_{32}B_U + c_{33}A_M + c_{34}B_M + c_{35}A_L + c_{36}B_L = 0 \quad (37)$$

$$c_{41}A_U + c_{42}B_U + c_{43}A_M + c_{44}B_M + c_{45}A_L + c_{46}B_L = 0 \quad (38)$$

$$c_{51}A_U + c_{52}B_U + c_{53}A_M + c_{54}B_M + c_{55}A_L + c_{56}B_L = 0 \quad (39)$$

$$c_{61}A_U + c_{62}B_U + c_{63}A_M + c_{64}B_M + c_{65}A_L + c_{66}B_L = 0 \quad (40)$$

in which, as before, the c_{ij} coefficients are defined by matching terms from equations (35)-(40) respectively with those of (29)-(34). But here there are many more coefficients that are zero, namely $c_{14}, c_{15}, c_{16}; c_{25}, c_{26}; c_{32}, c_{36}; c_{51}, c_{52}, c_{54}; c_{62}$. This greatly reduces the number of symbolic multiplies needed to apply Cramers rule, rendering it practical to work out all the algebra for this 6X6 system.

5.3. PARAMETER CHOICES AND SCANS

Equations (21)-(24) for the 2-layer model contain nine free parameters in addition to the poloidal forcing A_F ; equations (29)-(34) for the 3-layer model contain 16 parameters. Therefore we must make judicious choices of parameter values. In making these choices we will be guided by solar conditions as well as the uncertainties in the solar properties that define these parameters.

For example, the dimensionless frequency ω of the top forcing should be approximately the frequency of the solar cycle, corresponding to a period of 22 years. With η_U/H^2 our

frequency scale, for $\eta_U = 2 \times 10^{12} \text{cm}^2/\text{sec}$ and $H = 2 \times 10^{10} \text{cm}$ this frequency is $5 \times 10^{-9}/\text{sec}$. The solar cycle frequency is $9 \times 10^{-9}/\text{sec}$, so the dimensionless forcing frequency should be about 1.8 units. Therefore a frequency range of 1.5 to 2. would cover most variability in solar cycles. In all calculations displayed below, we have chosen a dimensionless frequency $\omega = 1.8$. Specifying the latitudinal wavenumber of the forcing is more uncertain. The width of the sunspot zone in one hemisphere is about 30 degrees latitude, or $\pi R/6$. This would be the minimum half wavelength of the forcing, but that forcing is seen to be broader in latitude scale than that, due to the dispersal and decay of active regions. Also, we never see surface fields from more than 2 sunspot cycles at the same time, so a more reasonable wavelength might be $\pi R/2$, the distance between equator and pole. Then this wavelength would correspond to a dimensionless wavenumber $k = 1.14$ units at the surface and $k = 1.63$ units at the depth of the tachocline. An average value would be about 1.4 units, which is what we use for all calculations. As for velocities, the velocity scale η_U/H is about 1m/sec, so a typical solar meridional flow near the top would be 15 units, and the latitudinal differential rotation linear velocity relative to the rotating frame of about $s = 70$ units.

We will use these dimensionless values to guide our choices of parameter ranges to survey. For some purposes the choice of $\eta_U = 10^{12} \text{cm}^2/\text{sec}$ may be too high. Reducing it by a factor of ten means that all dimensionless solar frequencies and velocities are increased by a factor of ten, but dimensionless wavenumbers remain the same.

6. 2 AND 3-LAYER RESULTS

6.1. ANALYTICAL EVIDENCE OF RESONANCE

The 1-layer results given above could give us guidance about where to look in parameter space for resonance when there are more layers than one. As in that case, we might expect that for resonance to occur in a layer, we must have the phase speed of the forcing at the top be equal to or vary close to the meridional flow speed in that layer. We have established both algebraically and numerically that resonance does happen in the bottom most layer of the system when the meridional flow satisfies that condition and the cross product of the coefficients of A_L and B_L approaches zero. In terms of formulas, this resonance occurs in the 2-layer model in the neighborhood of

$$c_{33}c_{44} - c_{34}c_{43} = 0 \tag{41}$$

and in the 3-layer model near where

$$c_{55}c_{66} - c_{56}c_{65} = 0 \tag{42}$$

In both 2 and 3-layer models this implies

$$\omega - kP_{vL}v_U = 0 \tag{43}$$

and

$$P_{\eta L}^2(k^2 + 6/D_L^2)(k^2 + 2/D_L^2) - \alpha_L^2(k^2 + 6/D_L^2) + \alpha_L s/2D_L = 0 \tag{44}$$

The fact that the conditions for resonance are identical in the 2 and 3-layer cases suggests that by induction that this will remain true no matter how many layers the model contains. Therefore it is likely to be a robust general property of this flux-transport dynamo, but we have not attempted to prove this mathematically. It is evident from equation (44) that the α -effect in the bottom layer plays an important role in creating resonance there. Some flux-transport models applied to the Sun contain no α -effect there, but Dikpati and Gilman (2001) showed that its presence could be responsible for choosing the correct symmetry for the Sun’s toroidal and poloidal fields (see also Bonanno et al 2002, Hotta & Yokoyama 2010). The resonance we demonstrate in this work gives further importance to knowing what the α -effect is at the base of the convection zone.

The conditions (43) and (44) guarantee an essentially infinitely large resonance (interestingly even though there is diffusion in the problem, which usually bounds the resonance to a finite value), but to be realized requires a precise combination of values of several parameters of the problem, very unlikely to be realized. But just being ‘close’ to resonance is enough to increase the response of the system to the same forcing at the top by a factor of 10-100, beyond the range of variation in solar cycle peaks. So it is worth mapping out the response over a wide range of parameter values that are plausible for the sun. But at the same time we must recognize that this 3-layer model is much simpler than the real sun, and much simpler than 2D flux transport dynamos in spherical shells.

Solutions of equation (44) in the limit of small $P_{\eta L}$ are of particular interest, since we expect the bottom layer to have the lowest magnetic diffusivity. In that limit the two roots are $\alpha_L = 0, sD_L/12$. In that case, there is resonance even if the α -effect is zero in the bottom layer.

6.2. NUMERICAL RESULTS FOR 2 AND 3 LAYER SYSTEMS

6.2.1. Location of resonance in parameter space

Here we answer the question of where in the parameter space we will find resonance occurring. In organizing the results it is helpful to differentiate roles played by the various parameters in the real sun, including how they might vary with either time or space. For example, while we do not know with precision the thickness of the bottom layer of the convection zone where we expect the magnetic diffusivity to be small, this thickness should not vary much with time, or probably with latitude. Therefore we can think of the thickness as an externally specified parameter. So we would like to know where in the range of other parameters resonance should occur, for a selection of assumed bottom layer thicknesses. Similarly, the solar differential rotation does not appear to vary much with time in the sun (the well-known torsional oscillations in rotation are about one-half of one percent of the equatorial rotation), so we can treat it in the same way.

The meridional flow varies more with time, but because of the density increase with depth, we expect the flow in the lower layer always to be much less than that of the upper layer and in the opposite direction. Somewhat arbitrarily we take the ratio of the two, $P_{v_L} = -0.1$. We also take the meridional flow of the middle layer to equal that of the upper layer, for simplicity and with some guidance from observations, e.g. Gizon and Rempel (2008), that do not show a reversal in meridional flow at mid-depth in the solar convection zone.

From theoretical considerations, we also do not expect the magnetic diffusivity in the bottom layer to vary with time, since it represents an average over many turbulent fluctuations; we do expect it to vary with depth, and this we have taken into account within the limitations of a 2 or 3 layer model. By contrast, the α -effect in the bottom layer may come from the action of a relatively small number of global events, such as global MHD instability, so it might fluctuate greatly with time, perhaps even changing sign. Therefore we choose to display our results as plots of the α -effect needed for resonance as a function of the other parameters.

Figure 2 displays α_L needed for resonance as a function of the magnetic diffusivity of the lower layer, for a solar differential rotation ($s = 70$) and a selection of lower layer thicknesses (the upper layer thickness is held fixed at 20% ($D_U = 0.2$) of the total thickness). Since the y-axis is logarithmic, we have reversed the sign of all the negative α_L values. Viewed from the left hand y -axis, the positive α_L values are the upper family of curves, while the negative α_L values are the lower family. The negative values are all asymptotic to zero with decreasing $P_{\eta L}$, while the positive values are all asymptotic to constant nonzero

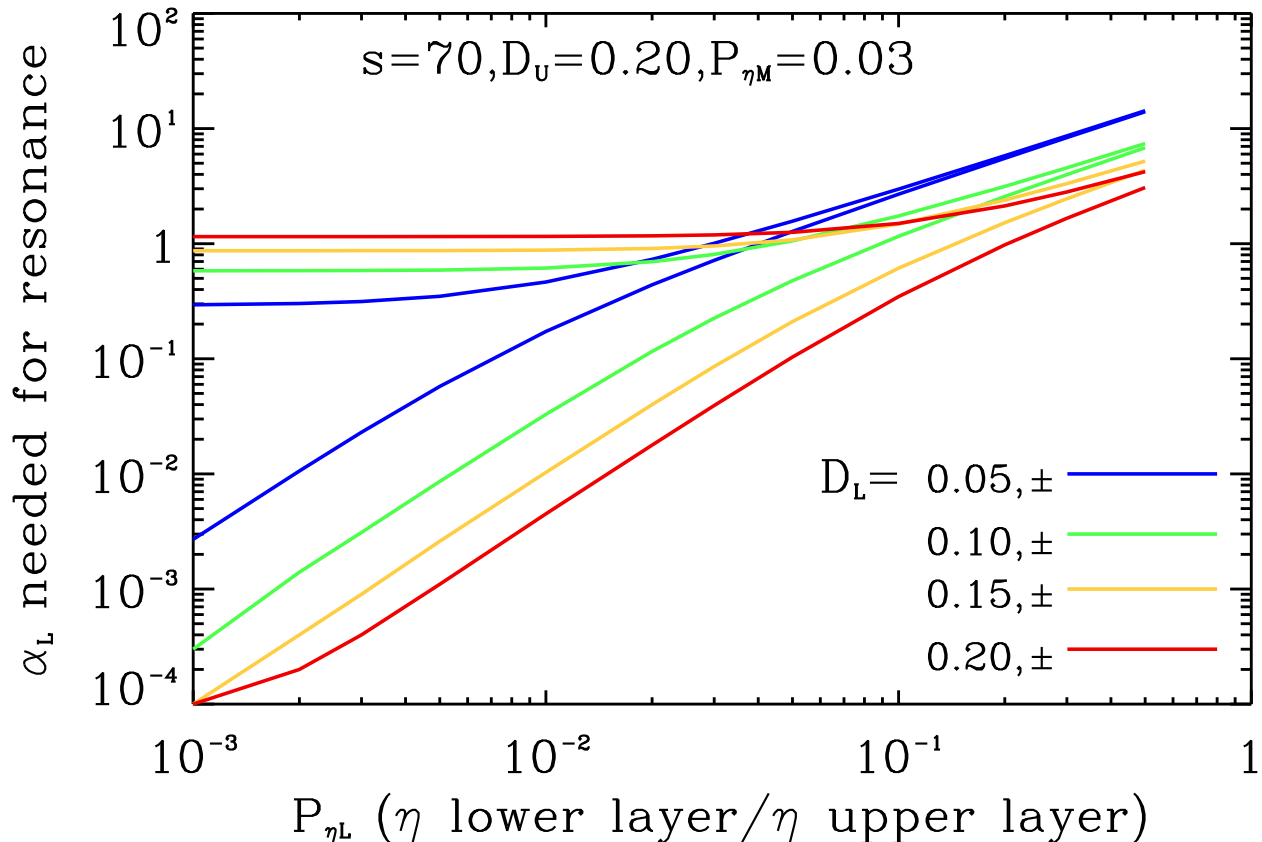


Fig. 2.— α_L needed for resonance as a function of lower layer diffusivity. All parameters are defined in the text. There are two values of α_L that give resonance for each lower layer thickness D_L (two curves of the same color). One is positive, the other negative (sign removed because of log scale used). Negative values asymptote to zero as lower layer diffusivity decreases (left hand edge of figure) while positive values asymptote to finite values.

values, consistent with the analytical limits shown in section 6.1. For increasing values of $P_{\eta L}$ the positive and negative α_L values for the same lower layer thickness are asymptotic to the same amplitudes, because in that limit the effect of differential rotation becomes insignificant. The effect of differences for different lower layer thicknesses also become less, because as the thickness increases, vertical diffusion shrinks to an amplitude closer to the latitudinal diffusion, which is proportional to k^2 , the square of the latitudinal wavenumber of the externally imposed forcing.

Figure 2 shows that for all lower layer magnetic diffusivities, there is always at least one $\alpha_L \sim O(1)$ available to create resonance, and two available if the lower layer diffusivity is high enough. This is true for all lower layer thicknesses shown, which cover the range

of reasonable values for the thickness of the layer with the lowest magnetic diffusivity in the dynamo domain ($1 - 4 \times 10^4 km$). A reasonable assumption for the Sun is that the turbulent magnetic diffusivity at the bottom is a factor $10^2 - 10^3$ smaller than at the top. With our scaling and the curves shown in Figure 2, this means resonance should occur for dimensional α_L values in the range $30 cm/sec - 1 m/sec$, which are very typical values used in flux-transport dynamos applied to the Sun. Resonance should also occur for much smaller values of α_L of the opposite sign.

We can give some physical interpretation of the results shown in Figure 2 and contained in the formulas used to generate it. There is a competition among the physical processes associated with the α -effect, magnetic diffusion, differential rotation and meridional circulation to determine where in parameter space resonance will occur. In general, diffusion works against resonance, while the α effect and differential rotation work to produce resonance by inductive processes. But, depending on their signs, the α -effect and differential rotation work with or against each other. From equation (44), if the product $\alpha_L s$ is negative they work in concert, and if it is positive, they are in opposition. We have taken s positive for the differential rotation, so when $\alpha_L < 0$ they reinforce, and when $\alpha_L > 0$ they oppose each other.

What happens is that oppositely signed α_L leads to oppositely directed poloidal potential and therefore oppositely directed toroidal fields induced by the same differential rotation. All patterns are swept toward the 'equator' by the meridional flow. In one case the induced toroidal field on the leading edge of the pattern reinforces what is already present, and in the other case it tends to cancel it out. Clearly the former case leads to a stronger response, or approach to resonance. This approach to resonance is optimized by choosing the meridional flow speed to match the forcing speed, effectively 'freezing' the phase of the forcing relative to the phase of the induced fields, allowing for maximum amplification.

When α_L and s are working together, for a given s , a smaller α_L is needed to achieve resonance. Hence for all diffusivities, the negative α_L values found for resonance are smaller in amplitude than their positive counterparts for the same values of other parameters, as seen in Figure 2.

The differential rotation value $s = 70$ in our scaling is equivalent to the whole differential rotation of the sun with latitude at the photosphere. But the lower layer of the model applies to the bottom of the convection zone and the tachocline, where the latitudinal differential rotation would be smaller by an amount that is a fairly strong function of depth. How much difference in the values of α_L that are needed to produce resonance occurs for lower differential rotation? Figures 3 and 4 give the answer.

In Figures 3 and 4 we display α_L needed for resonance as a function of the differential rotation parameter s , for the same lower layer thicknesses as shown in Figure 2, for two selected lower layer diffusivities $\eta_L = 6X10^9, 6X10^{10}cm^2/sec$ (Figures 3, 4 respectively), corresponding to $P_{\eta L} = 0.003, 0.03$, that cover the range of plausible values for the bottom of the solar convection zone. Here we use a linear scale for α_L so that we can retain its sign.

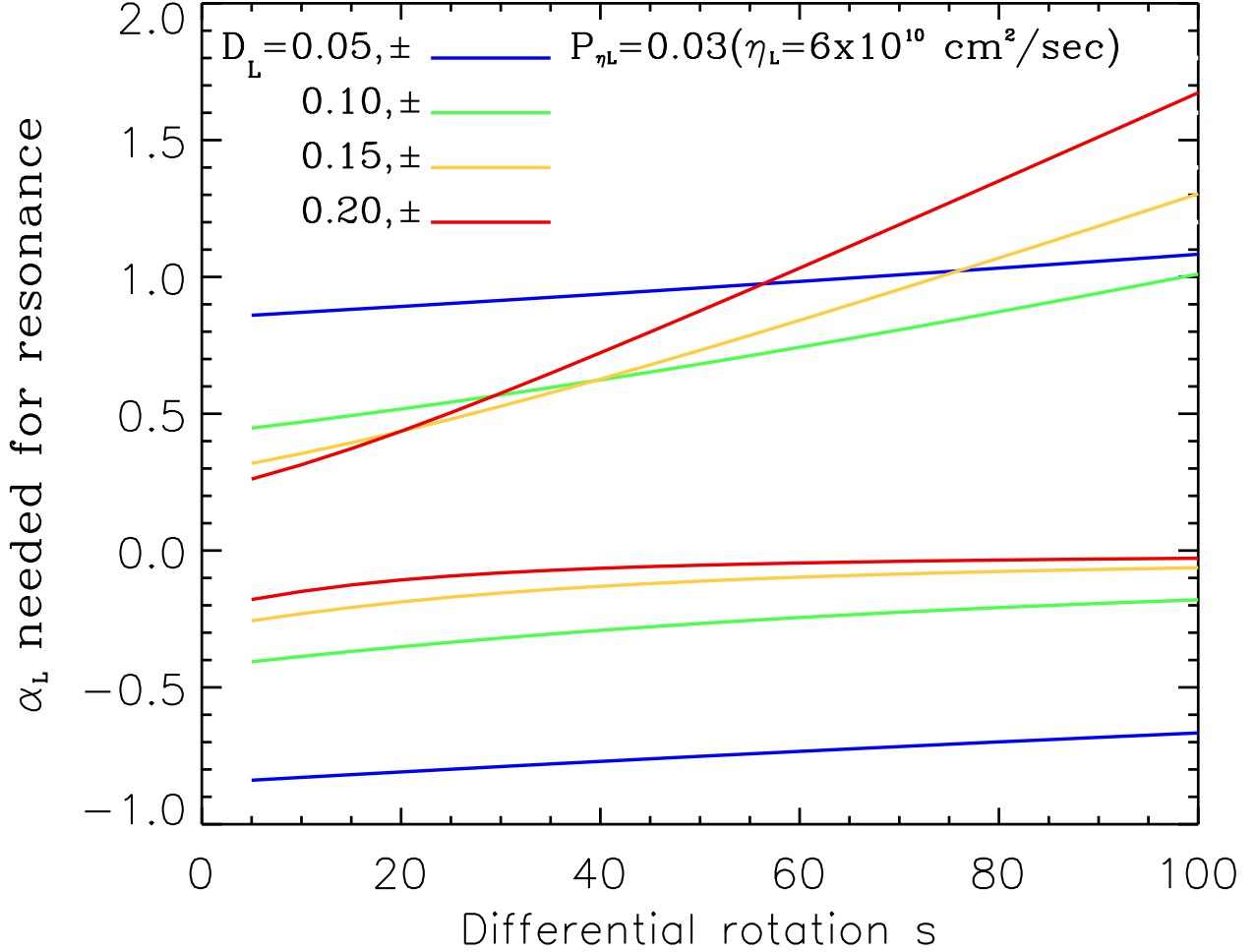


Fig. 3.— α_L needed for resonance as a function of the differential rotation parameter s for a lower layer magnetic diffusivity that is 0.03 of that of the upper layer. As in Figure 2, there are two α_L values, one of each sign (two curves of same color) for each lower layer thickness and choice of other parameters.

The primary message from Figures 3 and 4 is that, for lower layer thicknesses and diffusivities plausible for the Sun, resonance occurs for all differential rotations possible in the lower layer, for values of $\alpha_L \sim O(1)$. The positive α_L needed for resonance increases with differential rotation s , since in this case the α -effect and effect of differential rotation

oppose each other, while the negative α_L needed declines in amplitude with increase in s , because in this case the two effects reinforce each other.

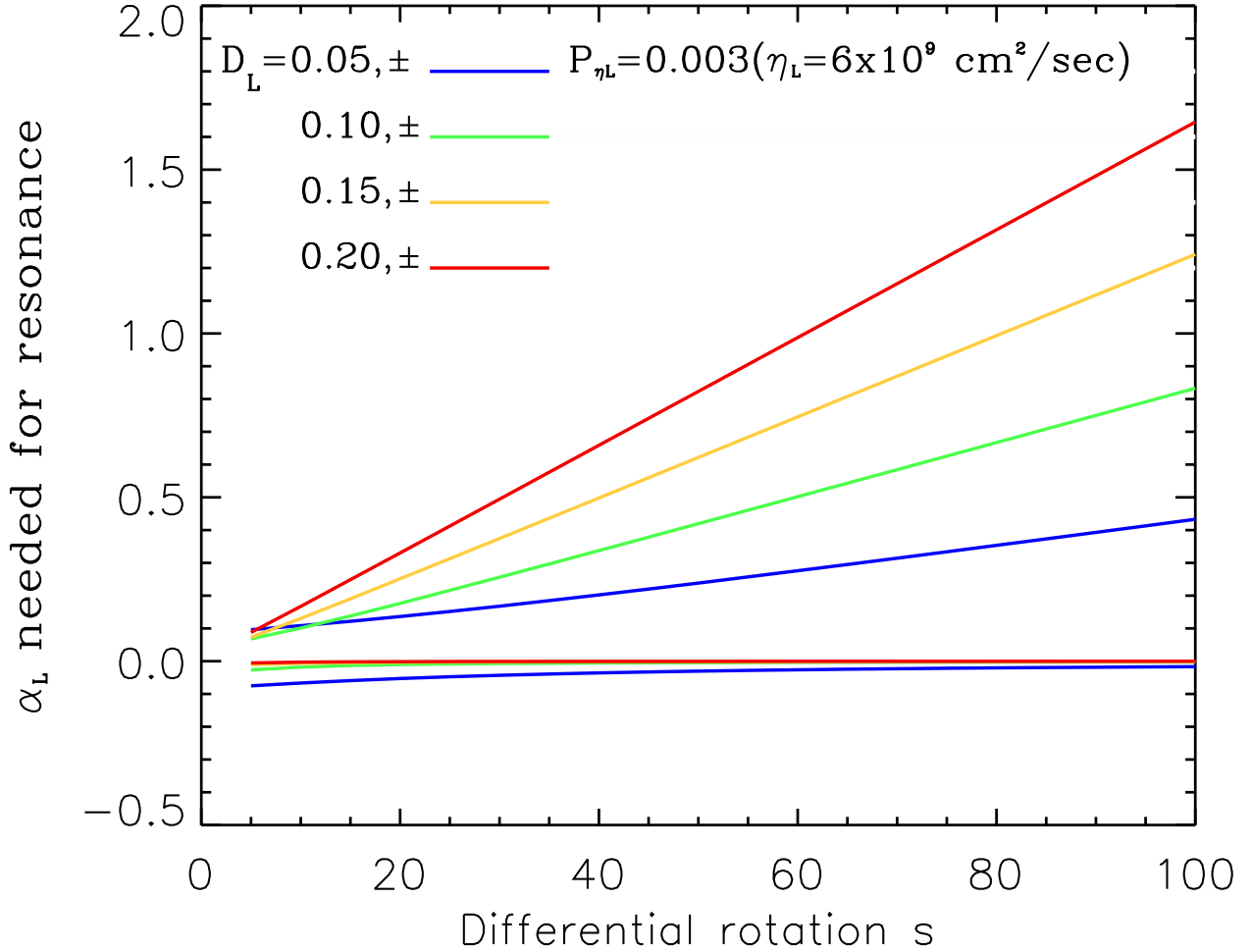


Fig. 4.— Same as Figure 3 but for a lower layer diffusivity that is 0.003 of that of the upper layer.

The results shown in Figures 2-4 apply to both two- and three-layer models, since equations (43) and (44) contain quantities only from the lower layer. But clearly the three-layer system captures more physics, so in the next section we focus on amplitude results for three layers. The corresponding results for two layers are qualitatively similar.

6.3. Examples of resonant response to forcing

The previous subsection presented guidance for where in our parameter space to find resonance. Here we present what that resonance looks like as functions of the various parameters of the problem. Figures 5 and 6 display the amplitudes of toroidal field and poloidal potential for all three layers of the model for poloidal forcing $A_F = 1$ for two selected lower layer magnetic diffusivities, the same as for Figures 3 and 4 respectively. These results are for full solar differential rotation ($s = 70$), a lower layer thickness of 10% of the total thickness, and a meridional flow speed at the top of $v_U = -12.86$, which is predicted from equation (43) for resonance in the lower layer for $\omega = 1.8$ and $k = 1.4$ when $P_{v_L} = -0.1$. It is important

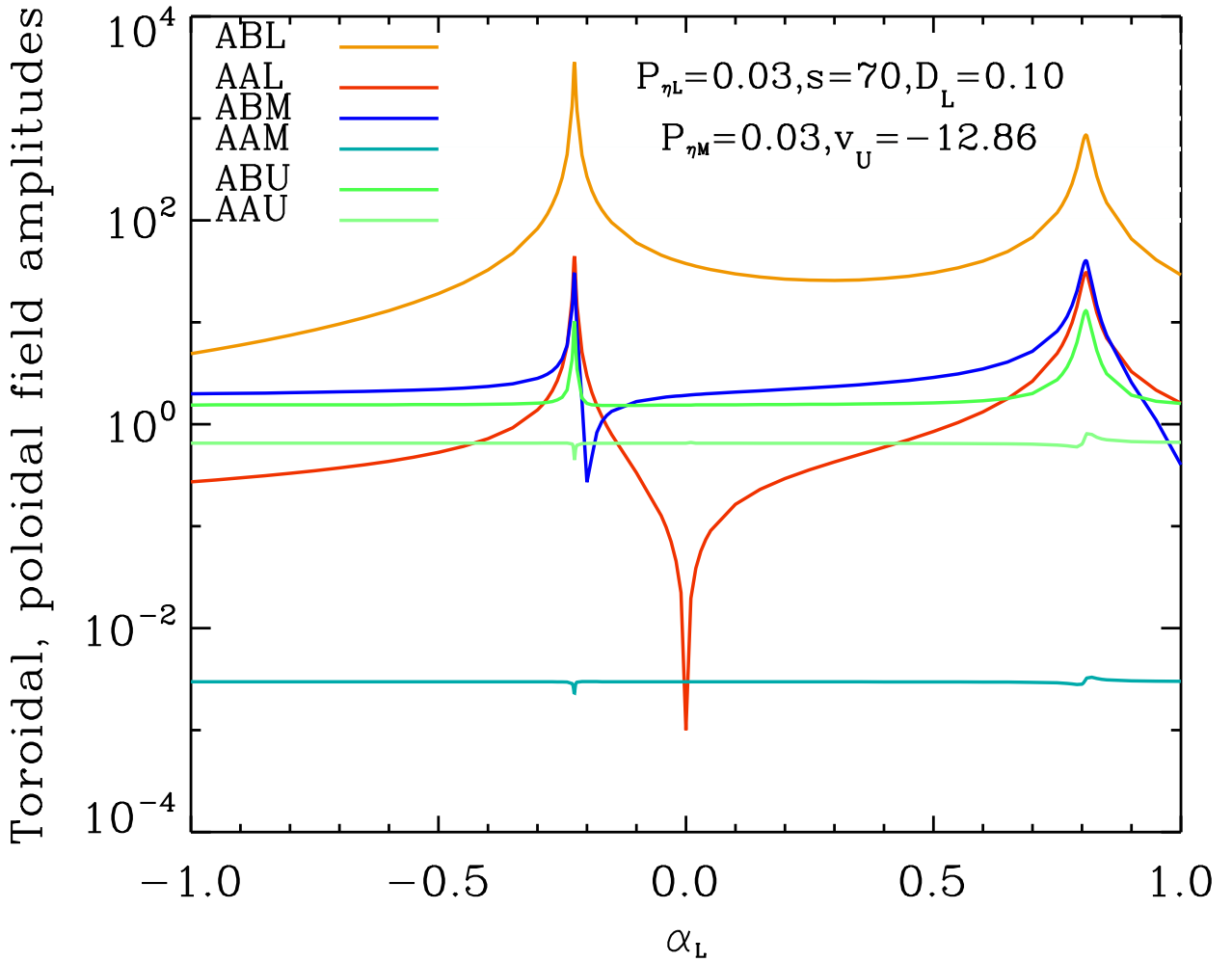


Fig. 5.— Toroidal and poloidal field amplitudes as functions of α_L for a lower layer magnetic diffusivity of 0.03 of that of the upper layer. Color key for all quantities shown in the upper left.

to realize that the amplitudes shown in Figures 5-7 are not exponentially growing as in the usual unforced dynamo solutions, but instead represent amplitudes of forced oscillatory solutions. Strictly speaking, these are not self excited dynamos, because of the top boundary forcing, but they are dynamos nonetheless. For these parameter values, equations (43) and

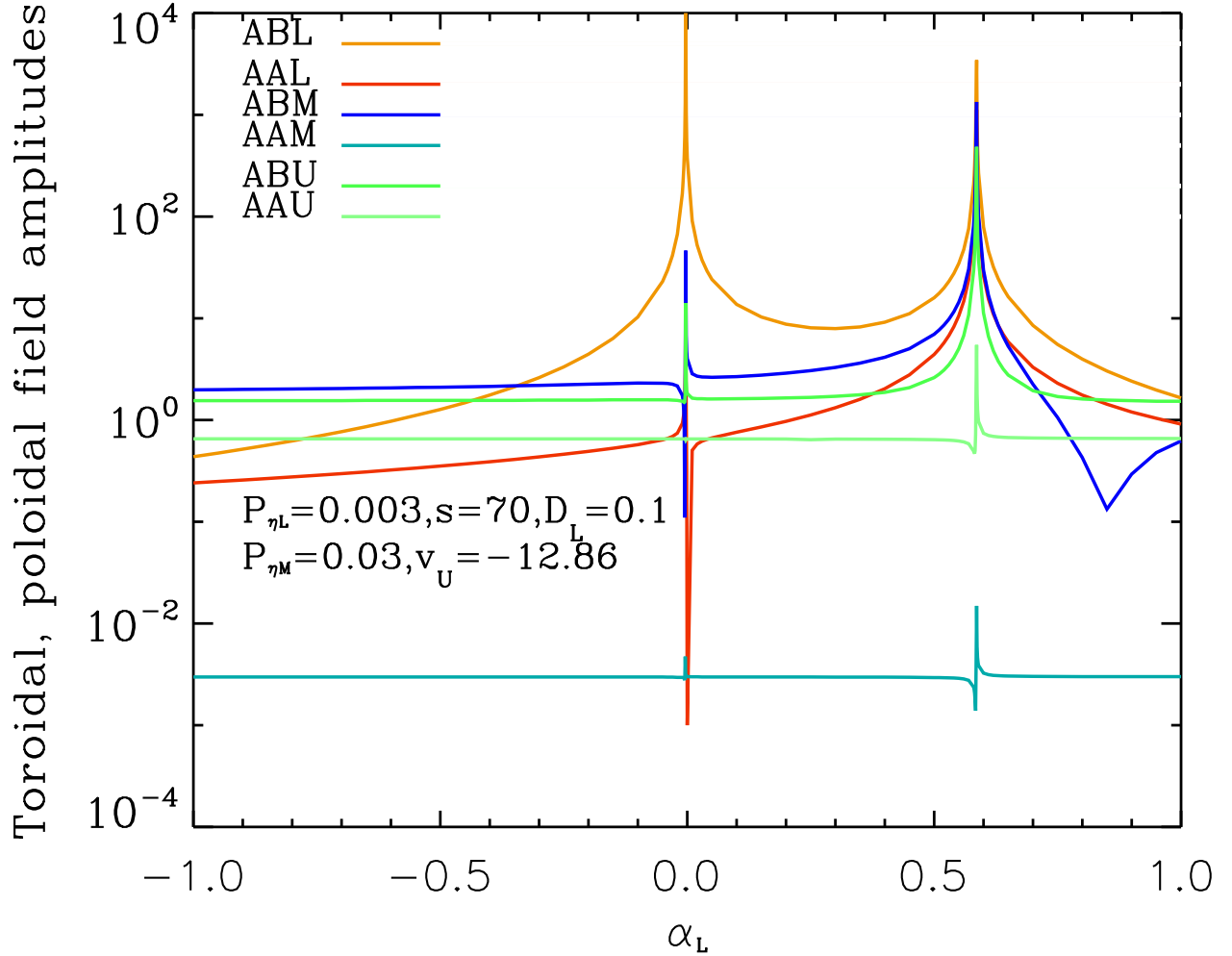


Fig. 6.— Same as in Figure 5 but for a lower layer magnetic diffusivity of 0.003 of that of the upper layer.

(44) predict resonance will occur near $\alpha_L = 0.807, -0.225$ for $P_{\eta L} = 0.03$ and $0.585, -0.003$ for $P_{\eta L} = 0.003$. We see strong upward spikes in *ABL*, the amplitude (absolute value) of the toroidal field in the lower layer (gold curve) at about these values of α_L . The lower layer poloidal potential *AAL* (red curve) also peaks there. Smaller peaks at the same α_L are present in the toroidal fields in the middle and upper layer (*ABM*, dark blue curve; *ABU*, dark green curve) while the poloidal potentials (*AAM*, light blue curve; *AAU*, light green

curve) of these layers respond to the resonance hardly at all. Finally, there is a downward spike in the poloidal potential of the lower layer at $\alpha_L = 0$. The poloidal potential of the upper layer is much larger than that of the middle layer because the former is determined directly by the forcing at the top, while in the middle layer only a small α_M is present.

Several features of Figures 5 and 6 are notable. We see in Figure 5 that for all values of α_L there is a large response in the lower layer, compared to the other layers, to the forcing applied at the top, even though the magnetic diffusivity in the lower layer is the same as that of the middle layer. This is because the meridional flow and the α of the middle layer are not close to the values needed for resonance in that layer. But at the same time, the middle and upper layers do show successively lower but still significant peaks in toroidal fields near the same values of α_L . This is caused by magnetic diffusion upward across the interfaces between layers.

The main changes seen in Figure 6 compared to Figure 5 are that with diffusivity of the lower layer reduced by a factor of ten, the resonance becomes much narrower and sharper. In other words, with lower diffusivity the range of α_L over which there is substantial amplification of the effect of the forcing at the top is narrower. But where resonance does occur, the middle and upper layers respond more strongly to the resonance for non-zero α_L . This is not true for the resonance near $\alpha_L = 0$, because such a low value leads to less production of poloidal field in the lower layer (compare the red curves in Figures 5 and 6 in the neighborhood of the resonance for negative α_L), from which the lower layer toroidal field must be produced by the differential rotation there.

Figures 5 and 6 are for a rather precisely chosen lower layer meridional flow speed. What happens to the resonance if we move away from that speed? We have examined this question by computing amplitudes of toroidal and poloidal fields as functions of α_L for other speeds, namely $v_U = -15, -14, -13, -12, -11$. We find the same resonances as seen in Figures 5 and 6, but with somewhat different amplification factors. Thus the presence of resonance of some significant amplitude is not strongly dependent on the precise value of the meridional flow. This means in effect that equation (44) more closely determines the resonance than does equation (43). In keeping with this inference, if we choose a value of α_L only a few percent away from that predicted to give resonance, the resonance practically disappears no matter what speed of meridional flow is taken.

Figure 7 displays the amplitude of the induced toroidal field in the lower layer as a function of meridional flow speed v_U in the upper layer, for the α_L values predicted for resonance for the same parameter choices as in Figures 5 and 6. We see that for $P_{\eta L} = .03$, the peak field does not occur at $v_U = -12.86$, at which equation (43) is satisfied, but rather at values above and below that (blue and green curves, respectively), depending on the α_L

pronounced for the parameter values chosen for Figure 5.

7. CONCLUSIONS AND DISCUSSION

Our principal conclusion is that, at least in this simple dynamo model, resonance will always be found, provided the right parameter values are chosen. Furthermore, it occurs for parameter choices that are plausible for the sun. It occurs in the lowest layer of the model, where the meridional flow toward the equator is most likely to match, or nearly match, the propagation speed of the forcing imposed at the top, corresponding to the photosphere on the sun. And the effect is large—a factor of 10-100 amplification of toroidal field compared to the case where the parameter values are far from the ones for which resonance is predicted. We acknowledge that this large a difference in amplitude for different parameter values is partly due to the model being kinematic. If jXB forces were included, the peaks would almost surely be smaller.

The solar convection zone is a spherical shell, not an infinite layer, so how well should we expect our results to apply to the Sun? In our model, the differential rotation s is a constant, so the rotation is a linear function of 'latitude' only, and independent of depth. In the Sun, differential rotation varies with both latitude and depth. In our model, meridional flow is independent of latitude, and there is no vertical motion, while in the Sun, meridional flow is a closed circulation confined by the boundaries of the convection zone as well as the poles. Meridional circulation is also known to vary with time on a variety of timescales. The α -effect will also be a function of latitude as well as time.

These differences between our model and the Sun imply that resonance, if it occurs, would likely be found in more localized regions of the dynamo domain. But in principle it could still occur. If a particular location experiences resonance or near resonance for some period of time, then the toroidal field might amplify quickly there, leading to locally anomalously large field. How quickly presumably depends on the nearness to conditions for resonance, and how long these conditions last. Could such a sudden amplification be a precursor for the formation of a rising flux tube that creates a new active region? This seems like a hypothesis worth testing in the future.

It is also possible that in the convection zone conditions for resonance could persist for large fractions of a solar cycle and perhaps even from one cycle to the next. If this happens, it could contribute to the evolution of the envelope of cycle amplitudes. On extremely long time scales could persistent conditions favoring resonance be responsible for 'grand maxima', and conditions unfavorable for resonance lead to 'grand minima', such as the Maunder

minimum? Clearly these are very speculative questions, requiring much more sophisticated solar dynamos than we have used here, to answer.

In flux-transport dynamos in spherical shells that are forced from the top, it is the radial flow of the closed meridional circulation that transports the forcing signal including its frequency to the bottom. In our infinite plane cartesian model, there is no radial flow, so the signal should be thought of as getting to the bottom locally via vertical diffusion and induction. We can think of the meridional circulation in the upper layer closing at infinity and returning in the lower layer.

Since we know that not all sunspot cycles have the same duration, the meridional flow will be bringing a frequency to the bottom that could be different than that implied by the meridional circulation there at the time the active regions were formed, that gave rise to the forcing frequency. Also, a change in the speed of the flow carrying the forcing signal will change the frequency of that signal by Doppler-shifting it. But in percentage terms the differences will not be large, so there could be continually evolving 'nearness' to conditions needed for resonance, creating continuous changes in cycle amplitude, in addition to the usual evolution of a sunspot cycle through ascending, peak, declining and minimum phases. Again, investigating such possibilities requires much more realistic dynamo models than we have used here.

The National Center for Atmospheric Research is sponsored by the National Science Foundation. This work is partially supported by the NASA Living with a Star Program through Award NNX08AQ34G.

REFERENCES

- Bonanno, A., Elstner, D., Rüdiger, G., & Belvedere, G. 2002, *A & A*, 390, 673
- Chiba, M. 1991, *MNRAS*, 250, 769
- Dikpati, M. & Charbonneau, P. 1999, *ApJ*, 518, 508
- Dikpati, M. & Gilman, P.A. 2001, *ApJ*, 559, 428
- Dikpati, M., de Toma, G., Gilman, P.A., Arge, C.N., & White, O.R. 2004, *ApJ*, 601, 1136
- Dikpati, M., Gilman, P.A. & MacGregor, K.M. 2005, *ApJ*, 631, 647
- Dikpati, M. & Gilman, P.A. 2006, *ApJ*, 638, 564
- Dikpati, M., Gilman, P.A., & de Toma, G. 2006, *GRL*, 33, L05102

- Fischer, M., Stefani, F. & Gerbeth, G. 2008, *Eur. Phys. J. B*, 65, 547
- Gizon, L. & Rempel, M. 2008, *Solar Phys.*, 251, 241
- Hotta, H., & Yokoyama, T. 2010, *ApJ*, 714, L308
- Kuzanyan, K.M. & Sokoloff, D.D. 1993, *Astrophys. Sp. Sci.*, 208, 245
- Moss, D. 1996, *A & A*, 308, 381
- Reshetnyak, M. 2010, arXiv:1009.2402v1
- Roald, C.B., 1998, *MNRAS*, 300, 397
- Schmitt, D. & Rüdiger, G. 1992, *A & A*, 264, 319
- Stefani, F. & Gerbeth, G. 2005, *Phys. Rev. Lett.* 94, 184506
- Strauss, H.R. 1986, *Phys. Rev. Lett.*, 57, 2231
- Ulrich, R. K. 2010, *ApJ*, 725, 658